Ordering of Brownian particles from walls due to an external force

Ordering of Brownian Particles from Walls Due to an External Force

Masahide Sato[a,*], Hiroyasu Katsuno[b], Yoshihisa Suzuki[c]

[a] *Information Media Center, Kanazawa University, Kakuma-machi, Kanazawa 920-1192, Japan*
[b] *Venture Business Laboratory,Nagoya University, Furo-cho, Chikusa-ku, Nagoya 464-8603, Japan*
[c] *Department of Life System, Institute of Technology and Science, The University of Tokushima, 2-1 Minamijosanjima, Tokushima, Tokushima 770-8506, Japan*

Abstract

Keeping the formation of colloidal crystal under a centrifugal force in mind, we study the ordering of Brownian particles under a uniform external force. Owing to the external force, the particles move in the direction of the external force. Near walls, the density of particles increases and the ordering of particles occurs on the walls at first. Then, the ordering in bulk proceeds gradually. Domains with the face-centered cubic and hexagonal close-packed structures are created in bulk. By controlling the direction and strength of external force, the ratio of the two types of structures changes.

Keywords: Brownian dynamics, colloidal crystal, centrifugal force,

1. Introduction

Colloidal crystals are three-dimensional regular structures formed by colloidal particles. With regard to the distance between particles, the colloidal

*Corresponding author: Tel: +81-76-234-6920; Fax: +81-76-234-6918
Email address: sato@cs.s.kanazawa-u.ac.jp (Masahide Sato)

crystals are classified into two types. One of them is non close-packed colloidal crystal, in which the distance between particles is longer than the radius of particles. One of their advantages is that the distance between particles is tunable, so they have very attractive features and are formed by various techniques [1–4]. Even in hard sphere system, when the density of particles is in a range [7–9], solidification occurs in order to decrease entropy. The transition is called as the Alder transition [5, 6]. In the recent study [9], the range of the volume fraction of hard spheres to cause the Alder transition is estimated to be 0.494-0.542 [9].

The other type of colloidal crystals is close-packed colloidal crystal, in which the distance between particles is as large as the size of particles. The close-packed colloidal crystals are widely noticed because they can be used as templates for inverse opals with perfect three-dimensional photonic bandgaps [10–12]. So far, many groups have tried to form large colloid crystals without defects [13–15]. In experiment [16], it was reported that the face-centered cubic(fcc) structure and the rhcp structure are mixed under normal gravity, although the random hexagonal close-packed (rhcp) structure is formed under microgravity. The experiment showed that the the gravity seems to enhance the formation of fcc structure, and the authors suggested that the enhancement of the formation of the fcc structure may be caused by stress. Recently, Hashimoto et al. [17] succeeded in creating a large close-packed colloidal crystal by a centrifugal method, using an inverted-triangle bottom container. They also created a close-packed colloidal crystal using a flat-bottomed container, and confirmed that the typical grain size of the colloidal crystal formed in the inverted-triangle bottomed container is larger

than that formed in the flat-bottomed container.

In Ref. [17], the authors suggested that the dependence of the typical grain size on the form of container is explained by the difference in nucleation rate. With a flat-bottomed container, nucleation of colloidal crystal occurs simultaneously in many places in bottom, The nucleus grow individually and a lot of columnar grains with narrow widths are formed. On the other hand, with an inverted-triangle bottomed container nucleation of grains mainly is limited near an edged bottom, and the grains of colloidal crystal are widen owing to the broadened sharp of the container.

In this paper, keeping the results of their experiment [17] in mind, we study the crystallization of Brownian particles. We carry out Brownian dynamics simulations with a uniform external force and investigate how the direction and strength of the uniform external force affect the time evolution of the crystallization. In Sec. 2, we introduce our model. In Sec. 3, we show the results of our simulation. In our previous studies [18, 19], we have not investigate how the time evolution of the two-dimensional ordering of particles on walls changes due to the strength of the external force. In this paper, we show the effect of the strength of an external force on the time evolution of the two-dimensional ordering on wall and numbers of particles with the fcc and the hcp structures. In Sec. 4 , we summarize our results and give brief discussions.

2. Model

We consider the system of a box with the size $L_x \times L_y \times L_z$. We use a periodic boundary condition in the y direction, and set walls in the x and

z directions. Initially, we put N particles in the system at random. Then, after moving the particles only with thermal noises for a long time, we add a uniform external force and start a simulation.

When the mass of the particles is m, the equation of motion of the ith particle is given by

$$m\frac{\mathrm{d}^2\boldsymbol{r}_i}{\mathrm{d}t^2} = \boldsymbol{F}_i - \zeta\frac{\mathrm{d}\boldsymbol{r}_i}{\mathrm{d}t} + \boldsymbol{F}_i^{\mathrm{B}}, \tag{1}$$

where $\boldsymbol{r}_i$ is the position of the ith particle, $\boldsymbol{F}_i^{\mathrm{B}}$ is the random force, $\boldsymbol{F}_i$ is the sum of an external force and internal forces from other particles, and ζ is the frictional coefficient. When the frictional force is very large, the inertial force, which is the term in the left side in eq. (1), is neglected. The velocity is approximately given by

$$\frac{\mathrm{d}\boldsymbol{r}_i}{\mathrm{d}t} = \frac{1}{\zeta}\left(\boldsymbol{F}_i + \boldsymbol{F}_i^{\mathrm{B}}\right). \tag{2}$$

We assume that the expected value of the random force $\langle\boldsymbol{F}_i^{\mathrm{B}}\rangle = \boldsymbol{0}$ and $\boldsymbol{F}_i^{\mathrm{B}}$ is related to ζ as $\left\langle F_{ix}^{\mathrm{B}}(t)F_{ix}^{\mathrm{B}}(t')\right\rangle = \left\langle F_{iy}^{\mathrm{B}}(t)F_{iy}^{\mathrm{B}}(t')\right\rangle = \left\langle F_{iz}^{\mathrm{B}}(t)F_{iz}^{\mathrm{B}}(t')\right\rangle = 2\zeta k_{\mathrm{B}}T\delta(t-t')$, where T is temperature and k_{B} is the Boltzmann constant. The force $\boldsymbol{F}_i$ is expressed as $\boldsymbol{F}_i = F_{\mathrm{ext}}\mathbf{e}_{\mathrm{ext}} - \sum_{i\neq j}\nabla U(r_{ij})$ where the first term is the external force by centrifugation and the second term is the sum of internal forces. F_{ext} and $\boldsymbol{e}_{\mathrm{ext}}$ represent the strength and unit vector parallel to the external force, respectively. $U(r_{ij})$ is the interaction potential between the ith and jth particles, where $r_{ij} = |\boldsymbol{r}_{ij}| = |\boldsymbol{r}_i - \boldsymbol{r}_j|$ is the distance between the two particles. As a interaction potential of colloidal crystal, the hard-sphere repulsion or a repulsive Yukawa potential may be better. However, from the experiment [17], the repulsion is probably short range, and we need to use a little more complicated algorithm more than that we explain

below in order to use a hard sphere potential [20]. Thus, for simplicity, we assume that the interaction between particles is a short-ranged repulsion, and use the Weeks-Chandler-Anderson potential [21] as the interaction potential. Namely, $U(r_{ij})$ is expressed as

$$U(r_{ij}) = \begin{cases} 4\epsilon\left[\left(\dfrac{\sigma}{r_{ij}}\right)^{12} - \left(\dfrac{\sigma}{r_{ij}}\right)^{6} + \dfrac{1}{4}\right] & (r_{ij} \leq r_{\rm in}), \\ 0 & (r_{ij} \geq r_{\rm in}), \end{cases} \tag{3}$$

where σ represents the characteristic size of particles and $r_{\rm in}$ is given by $2^{1/6}\sigma$. When the distance between two particles is smaller than $r_{\rm in}$, the two particles feel the repulsion from each other.

We use a simple model of Brownian dynamics. In our simulation, we use σ , $\zeta\sigma^2/\epsilon$, and ϵ/σ as the units of length, time, and force, respectively. The normalized difference equation of eq. (2) is expressed as [22] $\tilde{\boldsymbol{r}}_i(\tilde{t}+\Delta\tilde{t}) = \tilde{\boldsymbol{r}}_i(\tilde{t}) + \tilde{\boldsymbol{F}}_i\Delta\tilde{t} + \Delta\tilde{\boldsymbol{r}}_i^{\rm B}$, where $\tilde{\boldsymbol{r}}_i = \boldsymbol{r}_i/\sigma$ $\tilde{t} = t\epsilon/\zeta\sigma^2$ and $\tilde{\boldsymbol{F}}_i = \boldsymbol{F}_i\sigma/\epsilon$. The scaled displacement of the ith particle by random forces, $\Delta\tilde{\boldsymbol{r}}_i^{\rm B}$, satisfies $\left\langle \Delta\tilde{\boldsymbol{r}}_i^{\rm B}(t)\right\rangle = \boldsymbol{0}$ and $\left\langle \Delta x_i^{\rm B}(t)\Delta x_i^{\rm B}(t')\right\rangle = \left\langle \Delta y_i^{\rm B}(t)\Delta y_i^{\rm B}(t')\right\rangle = \left\langle \Delta z_i^{\rm B}(t)\Delta z_i^{\rm B}(t')\right\rangle = 2\tilde{R}^{\rm B}\Delta\tilde{t}$, where $\tilde{R}^{\rm B} = k_{\rm B}T/\epsilon$.

3. Results

First, we neglect the external force and carry out a simulation with a high density. The number of particles is 4000 and the volume fraction $4\pi(\sigma/2)^3/(3L_xL_yL_z)$ is 0.5, with which solidification occurs in a system with hard spherical particles. The strength of thermal noise $\tilde{R}^{\rm B}$ is 0.1. Figure 1 shows snapshots with a view from the y-direction, in which the positions of particles are drawn as points. Initially, the particles are put in the system

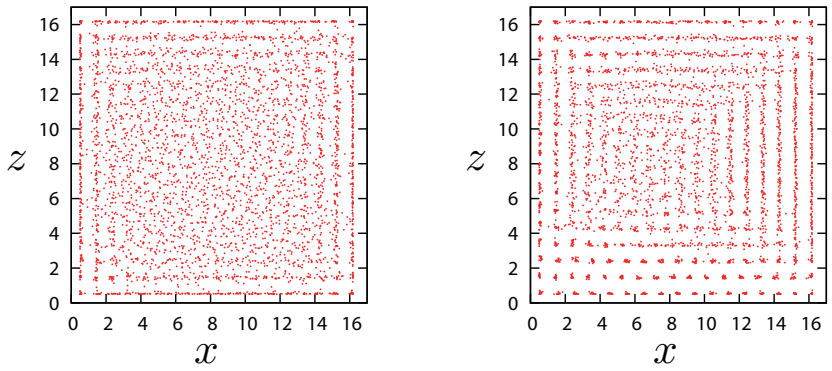

(a) (b)

Figure 1: (Color online) A snapshot of the positions of particles without an external force. $\Delta\tilde{t}$ is 1.0×10^{-3}. The times $\tilde{t}$ are (a) 4.0 and (b) 40.0.

at random. In an early stage (Fig. 1(a)), solidification starts from the neighborhood of walls and the layers parallel to the walls appear. In the late stage (Fig. 1(b)), the solidification proceeds in bulk and the width of the layers increases. The ordering in layers also occurs and the dotted pattern appears near the walls.

Then, we carry out simulations with 13500 particles with an external force. The system size is $L_x = L_y = L_z = 41.347$, so the volume fraction is 0.1. The volume fraction is enough low for solidification not to occur without the external force. In our simulation, Brownian particles act as hard spherical particles with the radius $r_{\rm in}/2$ against walls, and collide with the walls elastically. We move the particles without an external force in order to remove the dependence of the initial configuration, Then, we set the time $\tilde{t}$ to be 0 and start a simulation with an external force.

Figure 2 shows a snapshot of the positions of particles during a simulation. $F_{\rm ext}$ is 0.5 and $\boldsymbol{e}_{\rm ext}$ is $(1, 0, \sqrt{3})/2$. $\Delta\tilde{t}$ is 5.0×10^{-4}. The Peclet number

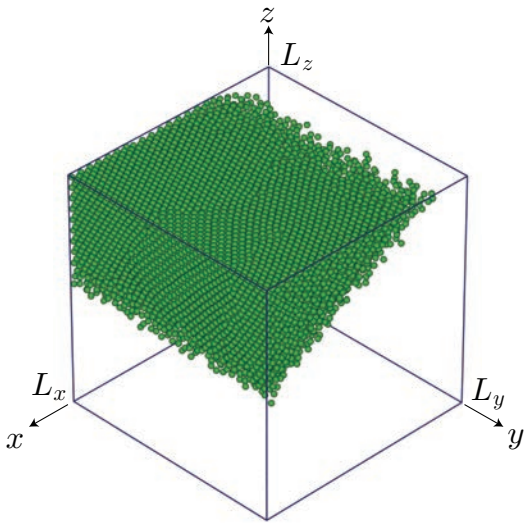

Figure 2: (Color online) A snapshot of the positions of particles with an external force. $F_{\rm ext}$ is 0.5 and $\boldsymbol{e}_{\rm ext}$ is $(1, 0, \sqrt{3})/2$. $\Delta\tilde{t}$ is 5.0×10^{-4}. The time $\tilde{t}$ is 6.0×10^{2}.

$P_{\rm e} = F_{\rm ext}\sigma/k_{\rm B}T = \tilde{F}_{\rm ext}/\tilde{R}^{\rm B} = 5$. The detail of process in crystallization has already reported in Ref. [18]. In an early stage, the particles are uniformly distributed in the system. Owing to the external force, the particles start moving to the direction of force, and the density in the upper left side increases. In later stage (Fig. 2), all particles gather in the upper left side. On the walls $x = L_x$ and $z = L_z$, the two-dimensional ordering of particles on the walls has already occurred.

To investigate the two-dimensional ordering of particles on a wall, we introduce the order parameter ψ_l, which shows a local sixfold orientation order around the lth particle. The definition of ψ_l is given by [23–26]

$$\psi_l = \frac{1}{n_l}\left|\sum_{m=1}^{n_l} \mathrm{e}^{6\mathrm{i}\theta_{l,m}}\right|, \tag{4}$$

where n_l is the number of neighboring particles of the lth particle. When the

distance between a wall and a particle is smaller than $r_{\rm in}/2$, we regard the particle as the particle attaching to the wall.

When both the lth and mth particles attach to the wall $z = L_z$ and the distance between them is smaller than a critical distance, we treat the mth particle as one of the neighboring particles of the lth particle. Taking account of thermal fluctuations, we use $1.1r_{\rm in}$ as the critical distance. In eq. (4), $\theta_{l,m}$ shows the angle formed by $(0, 1, 0)$ and the vector $(x_m - x_l, y_m - y_l, 0)$. When the two particles attach to the wall given by $x = L_x$, the vector $(x_m - x_l, y_m - y_l, 0)$ is replaced with $(0, y_m - y_l, z_m - z_l)$.

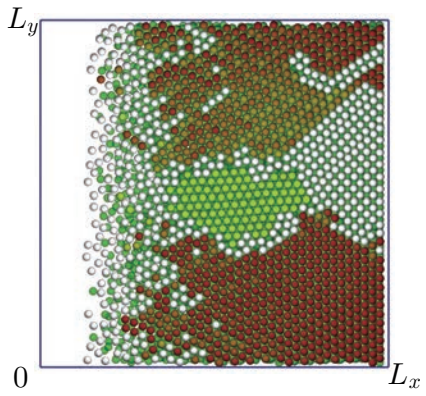

Figure 3: (Color online) A snapshot of the positions of particles on the top wall. The parameters are the same as those in Fig. 2. The time $\tilde{t}$ is 3.0×10^2.

Figure 3 shows a snapshot of the positions of particles in the top wall. The value of ψ_l of white particles is smaller than 0.9. When $\psi_l > 0.9$, the particles are colored and they form a triangular lattice. When one of the sides of the triangular lattice is parallel to $(0, 1, 0)$, the particles are colored red. With increasing angle between the side and $(0, 1, 0)$, the color gradually changes. When the angle is 30°, the color of particles becomes yellow. When

the particles do not attach to the wall, they are colored green. As reported in Ref. [18], initially, some particles attach to the top wall, but they are not ordered. With increasing time, the density of particles increases near the side edge between the two walls $x = L_x$ and $z = L_z$, and the particles start ordering around the edge. In late stage (Fig. 3), almost all the particles attaching to the wall form the square lattice or the triangular lattice.

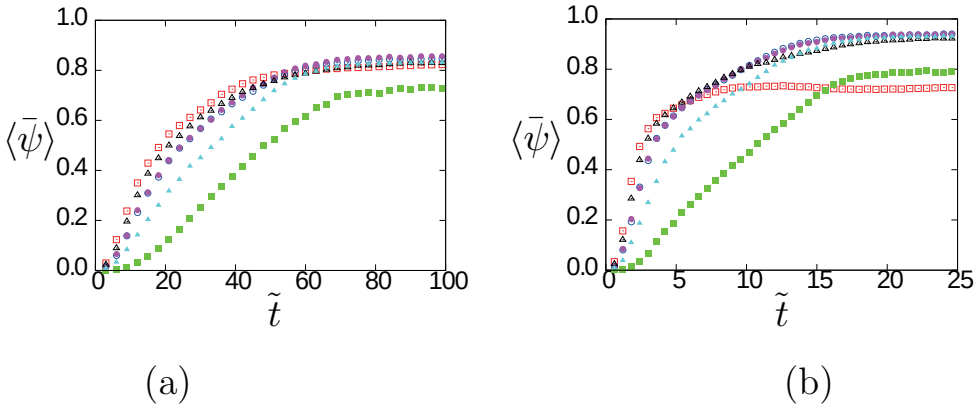

Figure 4: (Color online) Time evolution of $\langle\bar{\psi}\rangle$. The strength of an external force $F_{\rm ext}$ is (a) 0.5 and (b) $F_{\rm ext} = 2.0$. The tilting angles between the normal direction of a wall and the force direction are 0° with open squares, 30° with solid triangles, 45° with open and solid circles, 60° with open triangles, and 90° with solid squares. The data are averaged over 20 runs.

To study how the two-dimensional ordering of particles depends on the strength and direction of force, we investigate the time evolution of $\langle\bar{\psi}\rangle$, where $\bar{\psi}$ is the average of ψ_i on the whole of a wall in a run and an angle bracket represents the average over some individual runs. Figure 4 shows the time evolution of $\langle\bar{\psi}\rangle$ for various force directions, in which the data are averaged over 20 runs. The angle between the direction normal to the wall and that of the external force is defined as the tilting angle. Irrespective of

the force strengths and directions, $\langle\bar{\psi}\rangle$ increases with increasing time in an early stage. Then, the growth rate of $\langle\bar{\psi}\rangle$ becomes slow and $\langle\bar{\psi}\rangle$ is finally saturated. The growth rate in the initial stage increases with decreasing the tilting angle. When the force strength $F_{\rm ext}$ is 0.5 and the tilting angle is 90°, the saturation of $\langle\bar{\psi}\rangle$ occurs more slowly and the saturated value of $\langle\bar{\psi}\rangle$ is smaller than those with the other angles. When $F_{\rm ext}$ is 2.0 (Fig. 4(b)), the saturation of $\langle\bar{\psi}\rangle$ occurs much faster than that with $F_{\rm ext} = 0.5$. Expect for the time evolution with the tilting angle 0°, the saturated values of $\langle\bar{\psi}\rangle$ with $F_{\rm ext} = 2.0$ is larger than those with $F_{\rm ext} = 0.5$, and the forms of time evolution are similar to those with $F_{\rm ext} = 0.5$. When the tilting angle is 0°, the saturation of $\langle\bar{\psi}\rangle$ occurs faster than that with the other angles, and the saturated value of $\langle\bar{\psi}\rangle$ is smaller than that with the tilting angle 90°.

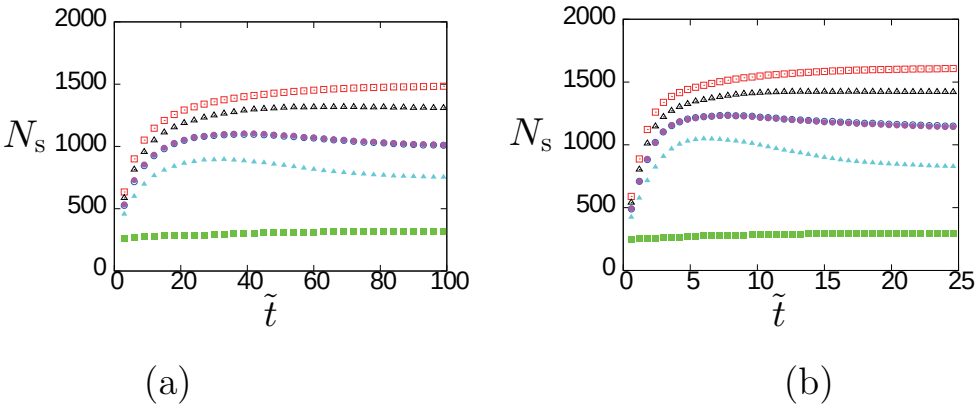

Figure 5: (Color online) Time evolution of the number of particles attaching to a wall with (a) $F_{\rm ext} = 0.5$ and (b) $F_{\rm ext} = 2.0$. The tilting angles between the normal direction of a wall and the force direction are 0° with open squares, 30° with solid triangles, 45° with open and solid circles, 60° with open triangles, and 90° with solid squares. The data are averaged over 20 runs.

We observe the number of particles attaching to walls and investigate its

relation to the ordering of particles on the walls. Figure 5 shows the time evolution of number of particles attaching to a wall. When the angles are 0° and 90°, the number of particles $N_{\rm s}$ increases monotonically. When the angles are 30° and 45°, the overshoot of $N_{\rm s}$ occurs in an early stage. We can find the overshoot more clearly in Fig. 5(b) than in Fig. 5(a). When $F_{\rm ext}$ is 2.0, the maximum of $N_{\rm s}$ appears at $\tilde{t} \simeq 5$, at which the increasing rate of $\langle\bar{\psi}\rangle$ starts slow in Fig. 4(b).

In our simulation, since the particles whose interaction is a short range repulsion are pressed by an external force, the expected structures in bulk are the hexagonal close-packed (hcp) and face centered cubic (fcc) structures. To find which structures dominantly appear in bulk, we introduce the parameters $Q_l(i)$ and $w_l(i)$ [18, 27–33], which represent the local orientation order in bulk around the ith particle. The parameter $Q_l(i)$ is defined as

$$Q_l(i) = \sqrt{\frac{4\pi}{(2l+1)} \sum_{m=-l}^{l} |q_{l,m}(i)|^2}, \tag{5}$$

where $q_{l,m}(i) = n_{\rm n}^{-1} \sum_{j=1}^{n_{\rm n}} Y_l^m(\theta_{ij}, \phi_{ij})$. The angles θ_{ij} and ϕ_{ij} represent the polar and azimuthal angles of $\boldsymbol{r}_{ij}$, respectively. $Y_l^m(\theta_{ij}, \phi_{ij})$ is the spherical harmonics and $n_{\rm n}$ is the number of neighboring particles around the ith particle. As in the calculation of ψ_k, we take account of the particles within $1.1r_{\rm in}$. The parameter $w_l(i)$ is defined as

$$w_l(i) = \frac{8\pi^{3/2}}{u(i)^{3/2}} \sum_{m_1+m_2+m_3=0} \begin{pmatrix} l & l & l \\ m_1 & m_2 & m_3 \end{pmatrix} q_{l,m_1}(i) q_{l,m_2}(i) q_{l,m_3}(i), \tag{6}$$

where $u(i) = (2l+1)Q_l(i)$. In eq. (6), the integers m_1, m_2 and m_3 run from $-l$ to l with satisfying the condition $m_1 + m_2 + m_3 = 0$, and the term in

the parentheses is the Wigner 3-j symbol [34]. We determine that the local structure of particles from Q_4-w_l plane [33]. The criterion we use is tighter than that used in Ref. [18]. The local structure is hcp structure when $0.06 < Q_4 < 0.14$ and $w_4 > 0.01$, and the fcc structure when $0.17 < Q_4 < 0.22$ and $w_4 < -0.01$.

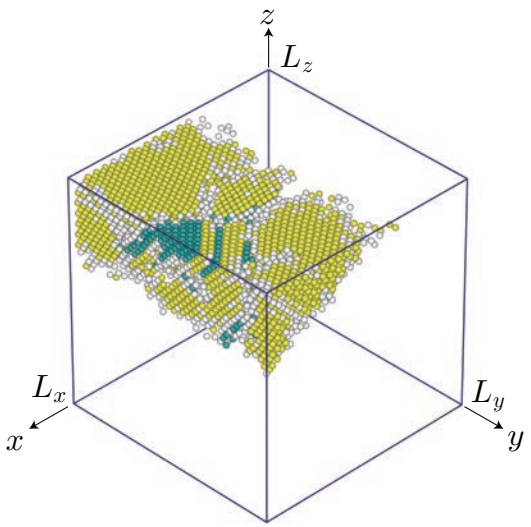

Figure 6: (Color online) A snapshot of the positions of ordered particles in bulk. The time $\tilde{t}$ is 6.0×10^2. Yellow particles, cyan particles, and white particles represent the particles with the hcp, fcc, and the other structures, respectively.

Figure 6 shows a snapshot of the local structure in bulk, where we use the data in Fig. 2 and draw he particles with 12 neighbors. Initially, there appear a few disordered particles near the edge formed by the walls $z = L_z$ and $x = L_x$. With increasing time, the number of particles with 12 neighbors increases and the ordering of particles starts near the edge. The particles have mainly the local hcp structure. In a late stage (Fig. 6), we find the particles with the fcc structure near the edge. As shown in Figs. 3, the particles with

the fcc structure appears under the square lattice formed on the wall $z = L_z$. Thus, the square lattice is one of the {100} faces of the fcc structure.

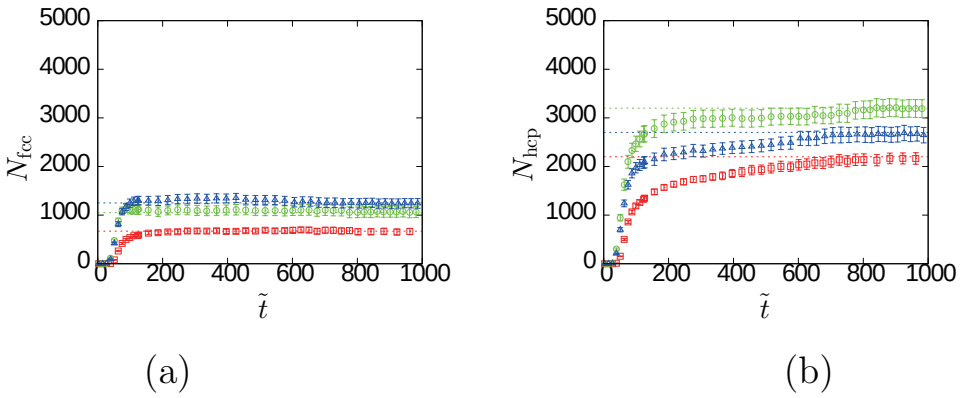

Figure 7: (Color online) Time evolutions of the number of particles with (a) fcc and (b) hcp structures. The force strength $F_{\rm ext}$ is 0.5. The force directions for squares, circles, and triangles are $(0, 0, 1)$, $(1, 0, 1)/\sqrt{2}$, and $(1, 0, \sqrt{3})/2$, respectively. The data are averaged over 20 runs.

We investigate how the time evolution of the numbers of ordered particles depends on the strength and direction of force. Figure 7 show the time evolution of the numbers of particles with the hcp and fcc structures $N_{\rm hcp}$ and $N_{\rm fcc}$, in which the force strength $F_{\rm ext}$ is 0.5. In the initial stage, the number of ordered particles increases with time. Then, the increasing rate decreases gradually, and the numbers of ordered particles saturate in a later stage. Comparing Fig. 7 with Fig. 4, we find that the three-dimensional ordering of particles in bulk proceeds slower than the two-dimensional ordering on walls. $N_{\rm fcc}$ and $N_{\rm hcp}$ saturate at $\tilde{t} \simeq 100$ and 800, respectively, so that the saturation of $N_{\rm fcc}$ is much faster than that of $N_{\rm hcp}$. Irrespective of the tilting angle, the saturated value of $N_{\rm hcp}$ is larger than that of $N_{\rm fcc}$. For the both structures, the saturated numbers of the ordered particles minimize when the external

force is perpendicular to a wall. The directions which give the maximum of the saturated value of $N_{\rm hcp}$ and $N_{\rm fcc}$ are $(1,0,1)/\sqrt{2}$ and $(1,0,\sqrt{3})/2$, respectively.

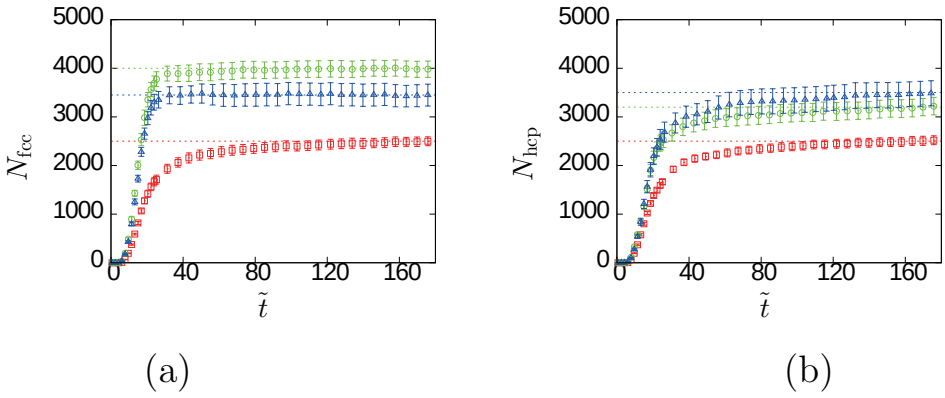

Figure 8: (Color online) Time evolutions of the number of particles with (a) fcc and (b) hcp structures. The force strength $F_{\rm ext}$ is 2.0. The force directions for squares, circles, and triangles are $(0,0,1)$, $(1,0,1)/\sqrt{2}$, and $(1,0,\sqrt{3})/2$, respectively. The data are averaged over 20 runs.

In Fig. 8, we use a large force ($F_{\rm ext} = 2.0$) and investigate how the time evolutions of $N_{\rm hcp}$ and $N_{\rm fcc}$ change. in which the force strength is 2.0. Comparing Fig. 7 with Fig. 8, we find that saturation of $N_{\rm hcp}$ and $N_{\rm fcc}$ occurs faster than those with the force strength 0.5. While the saturated values of $N_{\rm hcp}$ hardly change, the saturated values of $N_{\rm fcc}$ increase with increasing force strength. The directions which give the maximum of $N_{\rm fcc}$ and $N_{\rm hcp}$ are different from those with the force strength 0.5: the directions are $(1,0,1)/\sqrt{2}$ for $N_{\rm fcc}$ and $(1,0,\sqrt{3})/2$ for $N_{\rm hcp}$.

Figure 9 show the time evolution of the number of the ordered particles, which is the sum of $N_{\rm fcc}$ and $N_{\rm hcp}$. For all force directions, the saturated values with $F_{\rm ext} = 2.0$ are larger than those with $F_{\rm ext} = 0.5$. With both forces,

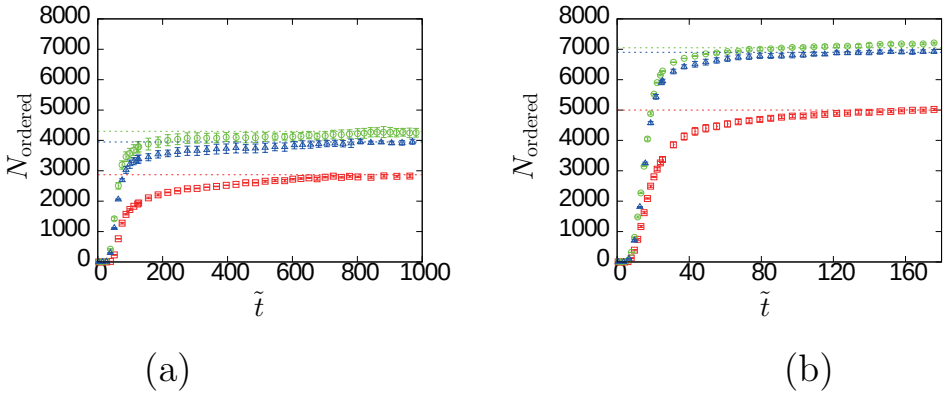

Figure 9: (Color online) Time evolutions of the sum of $N_{\rm fcc}$ and $N_{\rm hcp}$. The force strength $F_{\rm ext}$ is (a) 0.5 and (b) 2.0. The force direction for squares, circles, and triangles is $(0, 0, 1)$, $(1, 0, 1)/\sqrt{2}$, and $(1, 0, \sqrt{3})/2$, respectively.

the number of the ordered particles with the force direction $(1, 0, 1)/\sqrt{2}$ is larger than that with the force direction $(1, 0, \sqrt{3})/2$. However, the difference in the numbers of ordered particles caused by the two direction is small.

4. Summary

In this paper, we studied the time evolution of crystallization of Brownian particles under a uniform external force. For simplicity, we used high viscous approximation and neglect effects of hydrodynamic interaction between particles. Owing to the external force, the particles are moved to the direction parallel to the force and the ordering of particles on walls first occurs. Then, the ordering of particles in bulk occurs.

We investigated the dependence of the ordering of particles on the strength and direction of force. On the walls, the particles prefer to form a triangular lattice. The two-dimensional ordering becomes faster with increasing the force strength. When the force is small, the ordering with the force parallel

to the wall is smaller than that with the other force directions. However, with a strong force, the ordering of particles with the force normal to a wall becomes smallest.

The change of the dependence of the number of ordered particles on the force direction, which is caused by the change in the force strength, is explained by the velocity of sedimentation and the space on the walls. With a tilting force the density of particles increases from an edge. Near the other edge, there are sufficiently space on the wall and the layers of particles is thin. The particles can move their positions and triangular lattice is formed easily. On the other hand, when the force is normal to a wall and strong, the whole of the wall are simultaneously covered with the particles, which are pressed by the particles coming near the wall from behind. Thus, there is not sufficiently space for the particles to move to form a triangular lattice and the saturated value of order parameter becomes low with a strong force.

In bulk, the particles form the hcp and fcc structures. The numbers of the ordered particles, especially N_{fcc}, increase with increasing the force strength. With tilted forces, the numbers of ordered particles are more abundant than those with the normal force, which qualitatively agrees with a previous experiment [17]. As shown in Fig. 2, the crystal we obtained in our simulation is thin, so that the three-dimensional ordering in bulk strongly affects the two-dimensional ordering on walls. In our simulation, the two-dimensional ordering on walls with tilting forces is better than that with the normal force. Thus, the three-dimensional ordering in bulk with tilted forces become better than that with the normal force.

In our simulation, the domains with the local fcc structure and the local

hcp structure are mixed, which is probably because the external force and the density of particles are larger than the value used in previous studies [35–37]. In our simulation, the dependence of $N_{\rm fcc}$ and $N_{\rm hcp}$ on the tilting angle changes with change in the force strength, but now we cannot simply explain why the changes in $N_{\rm fcc}$ and $N_{\rm hcp}$ is caused by the difference in force direction, which is one of our future problems.

Acknowledgments

This work is supported by Grants-in-Aid for Scientific Research from Japan Society for the Promotion of Science, and some parts of this study was carried out under the Joint Research Program of the Institute of Low Temperature Science, Hokkaido University.

References

[1] T. Sawada, Y. Suzuki, A. Toyotama, and N. Iyi, Jpn. J. Appl. Phys. **40** (2001) L1226.

[2] T. Kanai, T. Sawada, A. Toyotama, and K. Kitamura, Adv. Funct. Mater. **15** (2005) 25.

[3] J. Yamanaka, M. Murai, Y. Iwayama, M. Yonese, K. Ito, and T. Sawada, J. Am. Chem. Soc. **126** 2004 (7156).

[4] A. Toyotama, J. Yamanaka, M. Yonese, T. Sawada, and F. Uchida, J. Am. Chem. Soc. **129** 2007 (3044).

[5] J.G Kirkwood, J. Chem. Phys., **7** 919 (1939).

[6] B. J. Alder and T. E. Wainwright, J. Chem. Phys. **27** (1957) 1208.

[7] P. N. Pusey and W. van Megen, Nature(London) **230** (1986) 324.

[8] W. G. Hoover and F. H. Ree, J. Chem. Phys. **49** (1968) 3609.

[9] R. L. Davidchack, and B. B Laird, J. Chem. Phys. **108** 9452 (1998)

[10] E. A. Kamenetzky, L. G. Magliocco, and H. P. Panzer, Science **263** (1994) 207.

[11] J. M. Weissman, H. B. Sunkara, A. S. Tse, and S. A. Asher, Science **274** (1996) 959.

[12] V. A. Blanco, E. Chomski, S. Grabtchak, M. Ibisate, S. John, S. W. Leonard, C. Lopez, F. Meseguer, H. Miguez, J. P. Mondia, G. A. Ozin, O. Toader, and H. M. Van Diel, Nature **405** (2000) 437.

[13] Y. Yin, Z. Li, and Y. Xia, Langmuir **19** (2003) 622.

[14] K. E. Davis, W. B. Russel, and W. J. Glantschnig, Science **245** (1986) 507.

[15] Y. Suzuki, T. Sawada, and K. Tamura, J. Cryst. Growth **318** (2011) 780.

[16] J. Zhu, M, Li, R. Rogers, W. Meyer, R. H. Ottewill, STS-73 Space Shuttle Crew, W. B. Russel, and P. M. Chaikin, Nature **387** (1997) 883.

[17] K. Hashimoto, A. Mori, K. Tamura, and Y. Suzuki, Jpn. J. Appl. Phys. **52** (2013) 030201.

[18] M. Sato, H. Katsuno, and Y. Suzuki Phys. Rev. E **87** (2013) 032403

[19] M. Sato, H. Katsuno, and Y. Suzuki J. Phys. Soc. Jpn. **82**, 084804 (2013).

[20] M. Marechal, M. Hermes, and M. Dijkstra, J. Chem. Phys. **135** (2011) 034510.

[21] J. D. Weeks, D. Chandler, and H. C. Anderson, J. Chem. Phys. **105** (1996) 9258.

[22] D. L. Ermak, J. Chem. Phys. **62** (1975) 4189.

[23] B. I. Halperin and David R. Nelson, Phys. Rev. Lett. **41** (1978) 121.

[24] R. Yamamoto and a. Onuki, J. Phys. Soc. Jpn. **66** (1997) 2545.

[25] R. Yamamoto and a. Onuki, Phys. Rev. E **58** (1998) 3515.

[26] T. Hamanaka and A. Onuki, Phys. Rev. E, **74** (2006) 011506.

[27] B. I. Halperin and D. R. Nelson, Phys. Rev. Lett. **41** (1978) 121.

[28] P. Steinhardt, D. R. Nelson, and M. Ronchetti, Phys. Rev. Lett. **47** (1981) 1297.

[29] P. J. Steinhardt, D. R. Nelson, and M Ronchetti, Phys. Rev. B **28** (1983) 784.

[30] M. D. Rintoul, and S. Torquato, J. Chem. Phys. **105** (1996) 9258.

[31] A. Panaitescu, K. A. Reddy, and A. Kudrolli, Phys. Rev. Lett. **108** (2012) 108001.

[32] W. Lechner and C. Dellago, J. Chem. Phys. **129** (2008) 114707.

[33] C. Desgranges and J. Delhommelle, Phys. Rev. B **77** (2008) 054201.

[34] L. Landau and E. Lifschitz, Quantum Mechanics, Pergamon, London, 1965.

[35] H. Mèguez, F. Meseguer, C. López, A. Misfud, J. S. Moya, and L. Vázquez, Langmuir **13**, 6009 (1997).

[36] P. Hoogenboom, D. Derks, P. Vergeer and A. van Blaaderen, J. Chem. Phys. 117, 11320 (2002).

[37] J. Hilhorset, J. R. Wolters, and A. V. Petukhov, Cryst. Eng. comm 12, 3820 (2010).